

Elastic properties of methane hydrate at high pressures

J. Baumert,^{1,2} C. Gutt,³ M. Krisch,⁴ H. Requardt,⁴ M. Müller,² J. S. Tse,⁵ D. D. Klug,⁵ and W. Press¹

¹*Institute Laue-Langevin, Grenoble, France*

²*Institut für Experimentelle und Angewandte Physik, Universität Kiel, Germany*

³*Experimentelle Physik I, Universität Dortmund, Germany*

⁴*European Synchrotron Radiation Facility, Grenoble, France*

⁵*Steele Institute for Molecular Science, National Research Council of Canada, Ottawa, Canada*

(Received 20 April 2005; published 16 August 2005)

The longitudinal acoustic phonon dispersion of high-pressure methane hydrate structures MH-II and MH-III was determined by *in situ* high-pressure inelastic x-ray scattering. These results on powder samples, in conjunction with the previously established equation of state, allowed the derivation of the aggregate compressional and shear sound velocity, as well as the effective elastic and shear modulus. The elastic properties were found to differ substantially from the elastic properties of high pressure ice structures, while strongly reflecting the transition from a cage clathrate (MH-II) to a filled ice structure (MH-III).

DOI: 10.1103/PhysRevB.72.054302

PACS number(s): 62.50.+p, 62.20.Dc, 63.20.Dj, 78.70.Ck

I. INTRODUCTION

Methane hydrate is an inclusion compound in which methane molecules are trapped in a host lattice of water molecules. The structure is thought to be stabilized by the repulsive interaction between the nonpolar guest and polar host molecules, which makes methane hydrate a model system for the study of hydrophobic interactions, relevant for the fundamental understanding of water potentials.¹ Furthermore, considerable interest has arisen as large natural accumulations of methane hydrate have been discovered on the oceanic sea floors, providing a potential future source of energy and an important factor in the global carbon cycle.² In addition, methane hydrate is thought to be a dominant constituent of the outer planets and their satellites.³ Recently, it has been suggested that the methane clouds on Titan, Saturn's largest moon, may be attributed to the formation of a stable high-pressure form of methane hydrate in the ice mantle.⁴ The mechanical properties of high-pressure forms of clathrate hydrates are therefore important parameters for the understanding of the geophysics in planetary systems. More specifically, our results are of direct relevance for the Cassini-Huygens mission, which recently succeeded to release the Huygens probe into Titan's atmosphere and impact it on the surface in order to collect data on the atmosphere and geological compositions.⁵

Three different crystallographic structures of methane hydrate are known today: a low-pressure phase I (MH-sI)⁶ and two high-pressure phases MH-II and MH-III.⁴ Methane hydrate structure I forms at moderate pressures (50–100 bar), whereas MH-II and MH-III form at about 10 and 20 kbar, respectively. At the structural phase transition from MH-II to MH-III, the cage structure of the hydrate collapses into a “filled ice” structure,⁷ where the guest molecules are found to occupy the channels of the ice network. This type of structure is also observed at high pressures for several other guest molecules or atoms.^{8,9} The details of the structures were found to depend strongly on the guest molecule. These range from a filled ice structure related to ice II or ice I_c for hy-

drogen guest molecules, to ice I_h in the case of methane guest molecules.

The low-pressure structure of methane hydrate was identified as the cubic structure type I of the clathrate family. The nominal stoichiometry is CH₄·5.75H₂O. The details of the crystallographic structure of MH-II are still unknown. Diffraction data could, however, be indexed by a hexagonal or primitive trigonal unit cell with lattice parameters close to those of clathrate structure type H.¹⁰ The structure of MH-III could be identified with a orthorhombic unit cell (space group Imcm). Both high-pressure structures are richer in methane than the low-pressure methane hydrate. Methane hydrate is the first clathrate found to exhibit a transformation from a cage clathrate to a filled ice. This transformation will undoubtedly lead to distinct changes in the dynamical properties of the hydrate and in the repulsive interaction between the nonpolar guest and the polar host molecules. Recent Raman scattering measurements revealed distinct changes of the C—H stretching mode of the methane molecules as a function of pressure: The change of the cage types from MH-sI to MH-II as well as the breakdown of the cage structure were observed.¹¹

In this paper, we present a study of the phonon dispersion curves of the high-pressure methane hydrate structures. High-energy resolution inelastic x-ray scattering (IXS) and diamond anvil cell (DAC) techniques were used to determine the orientationally averaged compressional sound velocities. Combining these findings with the results from diffraction experiments, the elastic properties of the high-pressure phases of methane hydrate were derived.

II. EXPERIMENTAL DETAILS

A MH-sI powder sample that was synthesized at the National Research Council, Canada, by condensing methane gas on a fine ice powder in a high pressure vessel,¹² was used to obtain the high-pressure methane hydrate structure. From previous experiments it is known that the MH-sI sample is contaminated by only a few percent of ice I_h.¹³ The x-ray

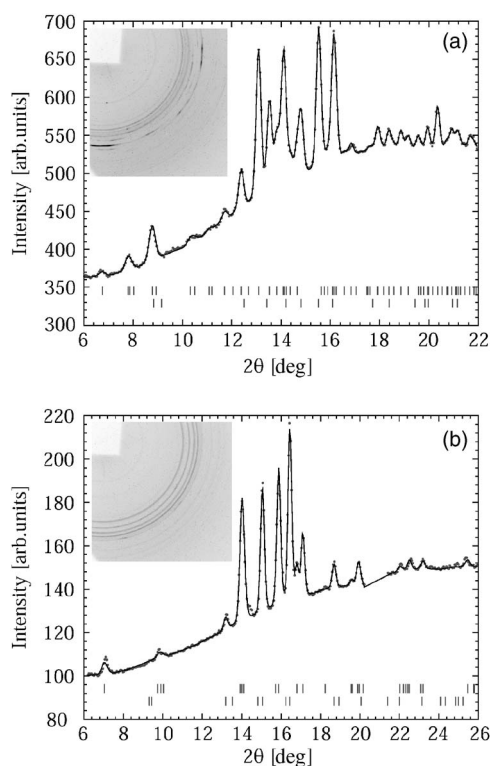


FIG. 1. Diffraction pattern of (a) the MH-II and (b) the MH-III sample at 17 and 21 kbar ($\lambda=0.697$ Å), respectively. The peaks are indexed for MH-II and MH-III (upper tick set) and ice VI (lower tick set), allowing for a profile matching (solid line).

experiments were performed at the IXS beam line ID28 at the European Synchrotron Radiation Facility in Grenoble. The instrument was operated at an x-ray energy of 17 794 eV ($\lambda=0.697$ Å), utilizing the Si (9 9 9) setup with an overall experimental energy resolution of 3 meV.

For the experiments, the powder sample was loaded at liquid nitrogen temperature into a DAC (culet size 600 μm , gasket hole diameter 400 μm , hole thickness 50 μm). The cell was sealed and then warmed to room temperature, leading to an initial pressure of about 11 kbar. The pressure was determined on-line using the ruby fluorescence method. At room temperature ($T=298$ K) the MH-II and MH-III were prepared by slowly raising the pressure to 17 and 21 kbar, respectively. The ice content of the samples after the structural phase transition can be deduced from the methane to water ratio of the different phases: MH-II has a 1:3.5 methane to water ratio ($\text{CH}_4 \cdot 3.5\text{H}_2\text{O}$),⁴ while the stoichiometry of MH-III is known to be $\text{CH}_4 \cdot 2\text{H}_2\text{O}$.⁷ Consequently, when the sample MH-sI is transformed into MH-II, the methane to water ratio changes from 8:46 to 10:35, leading to a high-pressure ice content of 39%. In the case of MH-III the ratio changes from 8:46 to 1:2, leading to 65% of high-pressure ice. At room temperature and pressures of 17 and 21 kbar, this leads to samples composed of both methane hydrate and ice VI.

Diffraction patterns of both the MH-II and the MH-III samples were recorded prior to the inelastic scans with a CCD detector. In Figs. 1(a) and 1(b) the integrated diffractograms and the CCD images (insets) of the MH-II and the

MH-III samples are shown, respectively. Using pattern matching, the peaks that are not attributed to ice VI could be indexed with the respective high-pressure methane hydrate phase confirming the sample composition. The MH-II diffractogram was indexed with a primitive trigonal unit cell [$a=11.833(1)$ Å, $c=9.955(1)$ Å] as proposed by Loveday *et al.*¹⁰ The integrated MH-III pattern was indexed with the space group Imcm [$a=4.770(4)$ Å, $b=8.067(5)$ Å, $c=7.964(5)$ Å] in agreement with the published results.⁷ Comparing the indexed diffraction patterns with the CCD images, it can be seen that for both samples the hydrate peaks correspond to uniform rings, while the strongest ice VI rings in the case of the MH-II sample display some irregularities. The uniform methane hydrate diffraction rings thus demonstrate that the hydrate samples are randomly oriented, nontextured powders.

III. EXPERIMENTAL RESULTS

A selection of inelastic x-ray spectra of the MH-II and MH-III samples at different wave vector transfers, or Q , between 2.0 and 8.9 nm^{-1} are shown in Figs. 2(a) and 2(b), respectively. The IXS data represent the orientationally averaged longitudinal acoustic dispersion, as no significant texture developed in the samples at the structural phase transitions, and as the large gasket hole ensured a sufficiently large number of crystallites within the scattering volume for a good powder average. The experimental data was normalized to the integrated intensity and the count rate at the central line was ~ 0.3 counts/s. In order to extract the energy positions $E(Q)$ of the inelastic excitations, the spectra were fitted using a pair of Lorentzian functions for each excitation, convoluted with the experimentally determined instrument resolution (solid line). The intensity ratio between the Lorentzian functions for both the energy loss and the energy gain is given by the Bose occupation factor. The instrument resolution is also shown in Fig. 2 (dashed line).

In the case of the MH-II sample, the energy positions of the inelastic excitations were determined to be $E=5.9$ meV, $E=15.8$ meV, and $E=22.5$ meV at $Q=2.0$ nm^{-1} . The two high-intensity peaks at $E=15.8$ meV and $E=22.5$ meV display strong dispersions and cannot be observed at wave vector transfers $Q > 5$ nm^{-1} . From the Q dependence of the energy positions of these two excitations, the sound velocities of ≈ 12 000 and ≈ 17 000 m s^{-1} are determined. These peaks are thus assigned to the transverse and longitudinal acoustic phonons of the diamond anvils.¹⁴ The third dispersive excitation is assigned to the orientationally averaged longitudinal acoustic (LA) phonon branches of the sample. As the sample is composed of 61% MH-II and 39% ice VI, this dispersive excitation at 5.9 meV, at $Q=2.0$ nm^{-1} , has contributions from the LA phonon branches of both ice VI and MH-II. For $Q \geq 6.9$ nm^{-1} , an additional nondispersive excitation is observed. Its energy position is found to be $E=11.9 \pm 0.2$ meV. It is tentatively assigned to transverse modes near the zone boundary, but it cannot be concluded whether it is due to phonons of ice VI or MH-II.

In the case of the MH-III at $Q=2.8$ nm^{-1} , three inelastic excitations with energy positions of $E=8.9$ meV,

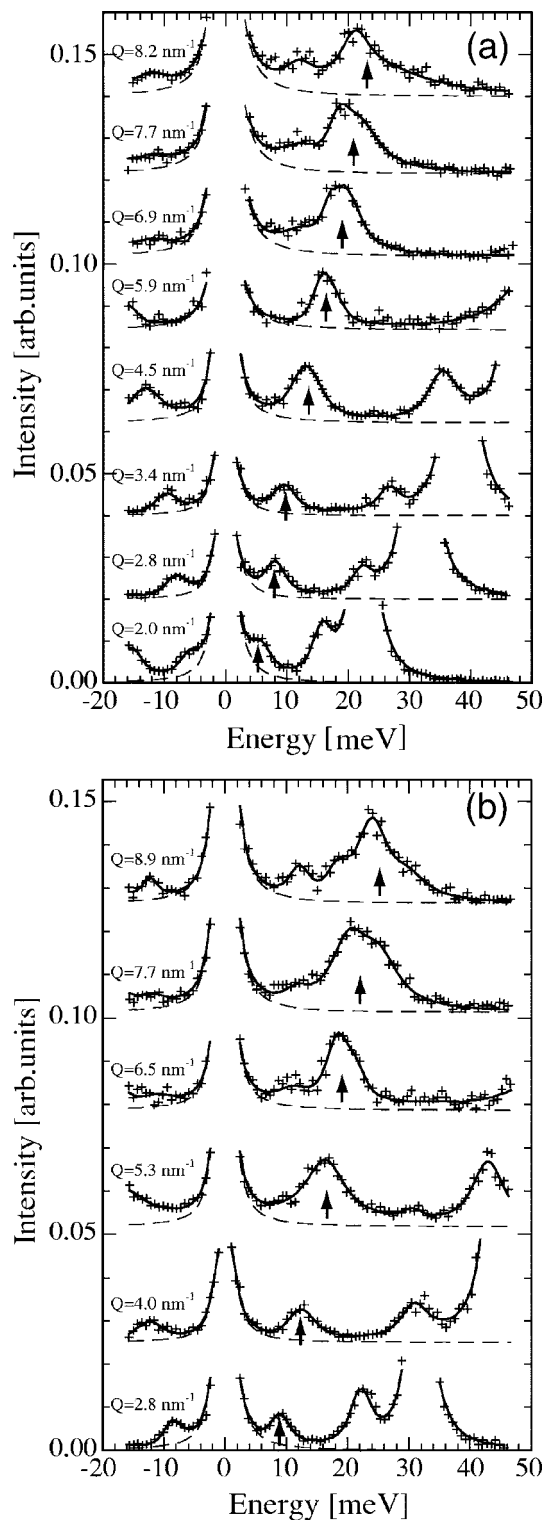


FIG. 2. Inelastic x-ray spectra of the (a) MH-II and (b) MH-III sample are shown for several Q values together with the fits (solid line) and the instrument resolution (dashed line). The two highly dispersive excitations are attributed to the acoustic phonons of diamond. The third dispersive excitation (see arrows) is assigned to the longitudinal acoustic phonons of MH-II or MH-III and ice VI. The LA phonons of methane hydrate and ice VI are visually distinguishable for $Q > 6.9 \text{ nm}^{-1}$ in the case of MH-II, and $Q > 6.5 \text{ nm}^{-1}$ for MH-III.

$E=22.2 \text{ meV}$, and $E=31.8 \text{ meV}$ can be observed. The two intense excitations at higher energies are, as in the case of MH-II, assigned to the acoustic phonons of the diamond anvils of the sample cell. As the sample is composed of 35% MH-III and 65% ice VI, the peak at 8.9 meV is assigned to the LA phonon branches of MH-III and ice VI. At $Q \geq 6.5 \text{ nm}^{-1}$, an additional excitation can be observed at $E \approx 12 \text{ meV}$. In the observed Q range this mode displays only a very weak dispersion and it is thus assumed to have a constant energy ($E=11.7 \pm 0.2 \text{ meV}$) within the experimental error. Additionally, at the highest displayed wave vector ($Q=8.9 \text{ nm}^{-1}$) a shoulder at $E \approx 18 \text{ meV}$ can be observed. The origin of the two additional excitations cannot be assigned unambiguously. Taking the relatively high momentum transfer into account, it is reasonable to assume that both are related to transverse phonons in either ice VI or MH-III.

The contribution of the ice VI/MH-II and ice VI/MH-III LA phonons to the IXS signal [see arrows in Figs. 2(a) and 2(b)] was disentangled by fitting two Lorentz functions. The energy position of the ice VI feature was initially set to values determined by Brillouin light scattering (BLS) results on polycrystalline ice VI.¹⁵ In the subsequent fitting iterations it was, however, allowed to vary to determine the energy positions of the hydrate and ice contributions simultaneously. A stable fit could be obtained for wave vector transfers $Q \geq 4.5 \text{ nm}^{-1}$ in the case of MH-II, since the line shape of the excitation becomes increasingly asymmetric with increasing Q . The excitation corresponding to the ice VI and MH-III LA phonons were separated in the same way, and a stable fit could be obtained for wave vector transfers $Q \geq 4.0 \text{ nm}^{-1}$. The intensity ratio between ice VI and MH-II was approximately 1:1.4, which corresponds to $\sim 58\%$ of MH-II in the sample. For the MH-III sample the ratio was found to be 2.1:1, corresponding to $\sim 32\%$ of MH-III in the sample. The intensity ratios determined from the fit of the experimental data thus agree with the sample composition derived from the results of diffraction experiments.

With the successful separation of the methane hydrate and ice contributions, the phonon dispersion curves for MH-II and ice VI at $p=17 \text{ kbar}$ [Fig. 3(a)] and MH-III and ice VI at $p=21 \text{ kbar}$ [Fig. 3(b)] could be obtained. The longitudinal, or compressional, velocities of sound were derived by fitting a sine law to the dispersion curves and determining the slopes in the $Q \rightarrow 0$ limit. For MH-II the first three points at momentum transfers of 2.0 , 2.8 , and 3.4 nm^{-1} were excluded from the fit, as a separation of the ice VI and MH-II LA phonons was not possible at these low Q values. In the case of MH-III the first point at $Q=2.8 \text{ nm}^{-1}$ was not taken into consideration. An orientationally averaged compressional sound velocity of $v_{\text{iceVI}}=4700 \pm 100 \text{ m s}^{-1}$ was determined for ice VI at $T=298 \text{ K}$ and $p=17 \text{ kbar}$. This value is in good agreement with values from BLS experiments ($v=4650 \text{ m s}^{-1}$).^{15,16} For MH-II an orientationally averaged compressional sound velocity of $v_{\text{MH-II}}=4200 \pm 100 \text{ m s}^{-1}$ was deduced from the phonon dispersion. For the MH-III sample the orientationally averaged compressional sound velocities at $p=21 \text{ kbar}$ and $T=298 \text{ K}$ are $v_{\text{iceVI}}=4950 \pm 100 \text{ m s}^{-1}$ and $v_{\text{MH-III}}=4600 \pm 100 \text{ m s}^{-1}$ for ice VI and methane hydrate MH-III, respectively. Again, the deduced sound velocity of ice VI is in good agreement with the values BLS experiments ($v=4900 \text{ m s}^{-1}$).

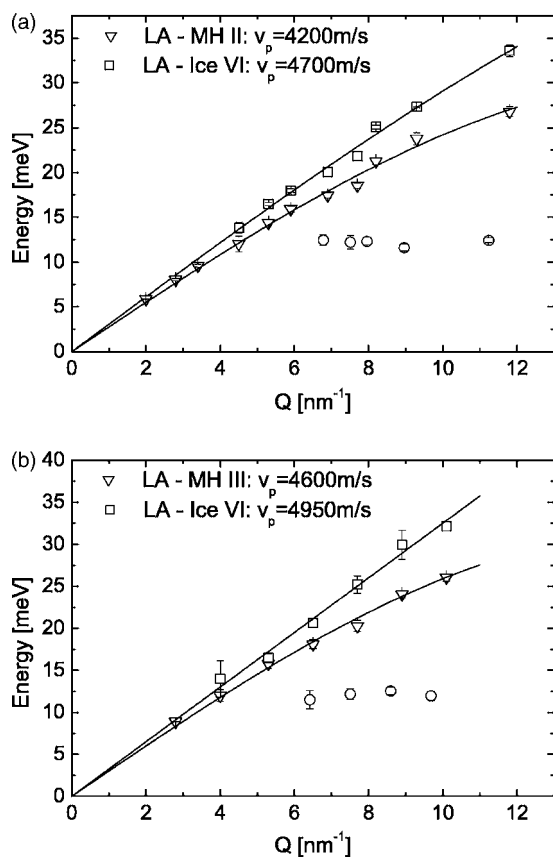


FIG. 3. Dispersion curve of (a) the MH-II sample at $p=17$ kbar and (b) the MH-III sample at $p=21$ kbar (open squares). They are shown together with the respective dispersion of ice VI (open triangles). The nondispersive mode at about 12 meV is reported for completeness as well (open circles).

For a randomly oriented, nontextured powder the compressional velocity of sound, which is the same as the orientationally averaged longitudinal sound velocity, is defined as $v_p = \sqrt{C/\rho}$, where C is a combination of the elastic constants (effective elastic modulus) and ρ the density of the material.¹⁷ On the other hand, the compressional and shear sound velocities can as well be expressed by $v_p = \sqrt{(1/\rho)(B + \frac{4}{3}G)}$ and $v_s = \sqrt{G/\rho}$, where B is the *bulk modulus* and G is the *shear modulus*. The pressure evolution of B and ρ are known from x-ray diffraction measurements. Consequently, as the samples were found to display good powder quality determined from the CCD diffraction data, C , G , and v_s can be derived from the experimentally determined longitudinal sound velocity v_p . The bulk modulus and the density of MH-II and MH-III are $B_{\text{MH-II}}=14.4$ GPa,¹⁸ $\rho_{\text{MH-II}}=1.07$ g cm⁻³ (Ref. 4) and $B_{\text{MH-III}}=23.6$ GPa, $\rho_{\text{MH-III}}=1.16$ g cm⁻³.⁴ We therefore obtain for MH-II $C=18.9\pm 0.8$ GPa, $G=3.4\pm 0.6$ GPa, and $v_s=1800\pm 150$ m s⁻¹. For MH-III we get $C=24.5\pm 1.0$ GPa, $G=0.8\pm 0.7$ GPa, and $v_s=800\pm 400$ m s⁻¹. Table I and Fig. 4 summarize the results for the three different ice clathrate phases. The moduli of MH-sI are taken from BLS results from Shimizu *et al.*¹⁹

TABLE I. Elastic properties of MH-II and MH-III summarized as deduced from the IXS measurements. Literature values for densities and bulk moduli as well as elastic properties of MH-sI (Ref. 19) are given for reference.

Hydrate pressure	MH-II 17 kbar	MH-III 21 kbar	MH-sI 0.2 kbar
ρ (g/cm ³)	1.07 (Ref. 4)	1.16 (Ref. 4)	0.90
B (GPa)	14.4 (Ref. 18)	23.5 (Ref. 4)	8.0
v_p (km/s)	4.2 ± 0.1	4.6 ± 0.1	3.7
C (GPa)	18.9 ± 0.8	24.5 ± 1.0	12.3
G (GPa)	3.4 ± 0.6	0.8 ± 0.7	3.3
v_s (km/s)	1.8 ± 0.15	0.8 ± 0.4	1.9

IV. DISCUSSION AND CONCLUSION

For the ambient pressure methane hydrate the influence of the guest molecules on the elastic lattice properties can be considered small in a first approximation. The inclusion of the methane guest molecules only leads to a small change in density of the water lattice compared to the density of the corresponding stable ice phase (ice I_h).²⁰ The difference in sound velocities can be explained by this change.²¹

This, however, is not true for the high-pressure hydrates MH-II and MH-III. In the case of MH-II the presence of the repulsive guest-host interaction prevents a denser structure comparable to the one of the stable ice phase (ice VI), leading to elastic constants, which are substantially smaller than those of ice VI. In fact, the elastic constants of MH-II are rather found to be similar to the ones of MH-sI. This is consistent with the suggestion that MH-II is a cage clathrate. However, in spite of the cage structure, MH-II does not show the anticrossing of the methane molecule phonon branches with the acoustic lattice phonons, observed in MH-sI.¹³ The growing repulsive interaction between the guest molecules and the host lattice of water molecules thus leads to the disappearance of the localized rattling motions of the methane molecules. For MH-III the elastic properties change consid-

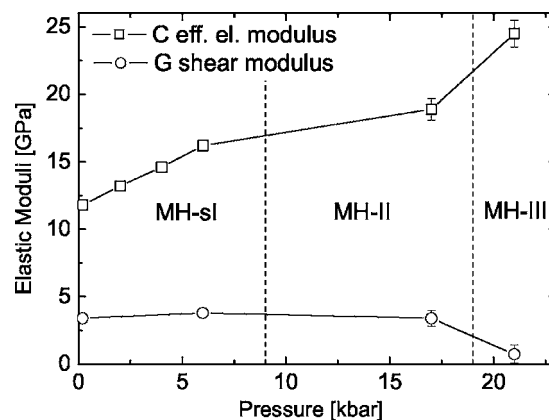


FIG. 4. The effective elastic modulus C and the shear modulus G , determined from the IXS experiments on MH-II and MH-III, are shown together with the pressure dependence of the elastic constants of MH-sI (Ref. 19). The lines are guides to the eye only.

erably. The effective elastic modulus is substantially higher than for MH-II, whereas the shear modulus decreases significantly. This behavior is consistent with a transition from a cage clathrate to filled-ice structure: the effective elastic modulus shows a strong increase that is attributed to the denser and more compact structure of MH-III. The decrease in the shear modulus can probably be related to the layered structure of ice sheets and nonpolar guest molecules. The repulsive interaction between the guest and host molecules is thus assumed to induce an instability to shear stress, having considerable consequences for the mechanical stability of MH-III bearing objects.

In summary, we have derived the first experimental values for the elastic properties of the high-pressure structures of methane hydrate, which show that the influence of the guest molecules is considerable at high pressures. It leads to elastic

properties, which are distinctly different from the ones of the stable ice phase at the same pressure. This should make the discrimination between high-pressure ice structures and hydrates easier and more accurate in future spectroscopic measurements. The presented results can be used for the identification and the theoretical modeling of these hydrate structures, and are potentially test cases for the understanding of water potentials.

ACKNOWLEDGMENTS

The authors thank Dean Gibson (ESRF) and Michael Hanfland (ESRF) for the assistance with the high pressure sample equipment. This work was funded by the BMBF and DFG within the program GEOTECHNOLOGIEN (Project No. 03GO551A, Publication no. GEOTECH-97).

-
- ¹K. Lum, D. Chandler, and J. D. Weeks, *J. Phys. Chem. B* **103**, 4570 (1999).
- ²E. D. Sloan, Jr., *Clathrate Hydrates of Natural Gases*, 2nd ed. (Marcel Dekker Inc., New York, 1998).
- ³J. I. Lunine and D. J. Stevenson, *Icarus* **70**, 61 (1987).
- ⁴J. S. Loveday, R. J. Nelmes, M. Guthrie, S. A. Belmonte, D. R. Allan, D. D. Klug, J. S. Tse, and Y. P. Handa, *Nature (London)* **410**, 661 (2001).
- ⁵<http://saturn.jpl.nasa.gov/home/index.cfm>
- ⁶D. W. Davidson, Y. P. Handa, C. I. Ratcliffe, J. S. Tse, and B. M. Powell, *Nature (London)* **311**, 142 (1984).
- ⁷J. S. Loveday, R. J. Nelmes, M. Guthrie, D. D. Klug, and J. S. Tse, *Phys. Rev. Lett.* **87**, 215501 (2001).
- ⁸W. L. Vos, L. W. Finger, R. J. Hemley, and H. K. Mao, *Phys. Rev. Lett.* **71**, 3150 (1993).
- ⁹C. Lobban, J. L. Finney, and W. F. Kuhs, *J. Chem. Phys.* **117**, 3928 (2002).
- ¹⁰J. S. Loveday, R. J. Nelmes, and M. Guthrie, *Chem. Phys. Lett.* **350**, 459 (2001).
- ¹¹H. Shimizu, T. Kumazaki, T. Kume, and S. Sasaki, *J. Phys. Chem. B* **106**, 30 (2002).
- ¹²Y. P. Handa and J. G. Cook, *J. Phys. Chem.* **91**, 6327 (1987).
- ¹³J. Baumert, C. Gutt, V. P. Shpakov, J. S. Tse, M. Krisch, M. Müller, H. Requardt, D. D. Klug, S. Janssen, and W. Press, *Phys. Rev. B* **68**, 174301 (2003).
- ¹⁴M. H. Krisch, A. Mermet, A. San Miguel, F. Sette, C. Masciovecchio, G. Ruocco, and R. Verbeni, *Phys. Rev. B* **56**, 8691 (1997).
- ¹⁵A. Polian and M. Grimsditch, *Phys. Rev. B* **27**, 6409 (1983).
- ¹⁶H. Shimizu, T. Nabetani, T. Nishiba, and S. Sasaki, *Phys. Rev. B* **53**, 6107 (1996).
- ¹⁷E. Schreiber, O. Anderson, and N. Soga, *Elastic Constants and their Measurement* (McGraw-Hill, New York, 1973).
- ¹⁸H. Hirai, Y. Uchihara, H. Fujihisa, M. Sakashita, E. Katoh, K. Aoki, K. Nagashima, Y. Yamamoto, and T. Yagi, *J. Chem. Phys.* **115**, 7066 (2001).
- ¹⁹H. Shimizu, T. Kumazaki, T. Kume, and S. Sasaki, *Phys. Rev. B* **65**, 212102 (2002).
- ²⁰R. E. Gagnon, H. Kiefte, M. J. Clouter, and E. Whalley, *J. Chem. Phys.* **89**, 4522 (1988).
- ²¹E. Whalley, *J. Geophys. Res.* **85**, 2539 (1980).